Application of seismic interferometry by multidimensional deconvolution to crosswell seismic reflection using singular-value decomposition

S. Minato , T. Matsuoka and T. Tsuji, Kyoto University, D. Draganov, Jürg Hunziker and K. Wapenaar, Delft University of Technology*

Summary

Seismic interferometry is a process of generating new seismic data from existing wavefields. This enables us to expand the degree of freedom of source-receiver configuration. Seismic interferometry by multidimensional deconvolution (MDD) is proposed as an alternative to the conventional crosscorrelation method (Wapenaar et al., 2008a; Wapenaar et al., 2008b). We apply MDD to crosswell geometry in order to retrieve crosswell impulse responses from surface sources using numerical modeling and field data. We adopted singular-value decomposition (SVD) for obtaining the pseudoinverse solution to achieve MDD. Since the SVD pseudoinverse is highly dependent on the rank of the MDD matrix, Akaike's information criterion (AIC) is adopted in order to determine the rank of the MDD matrix. We see that the MDD produces higher-resolution data compared with the conventional crosscorrelation method. Furthermore, amplitudes of downgoing reflection events are improved in MDD while downgoing reflection events are not recognizable in the crosscorrelation method.

Introduction

Seismic interferometry can be defined as the process of generating new seismic data from the crosscorrelation of existing wavefields from controlled sources around receivers of interest. The literature on interferometric techniques has grown spectacularly in recent years (e.g., Wapenaar et al., 2004; Wapenaar et al., 2006; Schuster et al., 2004; Snieder 2004; Bakulin and Calbert 2006). We have studied the application of seismic interferometry to crosswell geometry (Minato et al., 2007). In this application, the receiver arrays are placed in vertical boreholes and the controlled sources are placed along the surface. From this configuration, crosswell wavefields can be retrieved using seismic interferometry. Therefore, there is a possibility to perform crosswell seismic reflection without physical borehole sources. Furthermore, this method enables us to expand the investigation area using high-energy sources on the surface.

Recently, seismic interferometry by multidimensional deconvolution (MDD) has been proposed as an alternative to the conventional crosscorrelation method (Wapenaar et al., 2008a; Wapenaar et al., 2008b). Advantages of seismic interferometry by MDD are that it compensates for the characteristics of the source wavelet, that may compensate for inhomogeneous source distribution, and that it is valid in dissipative media (the crosscorrelation method assumes lossless medium).

In this study, we show that the crosswell seismic reflection method can be performed without borehole sources using seismic interferometry by MDD and that the amplitudes and resolution of imaged reflection boundaries are improved compared with results from the conventional crosscorrelation method. These applications were examined using numerical modeling and field data. Because our source-receiver configuration was an ill-posed problem for solving interferometry relation, we adopted an SVD pseudoinverse solution to achieve multidimensional deconvolution. Furthermore, we applied AIC (Akaike's information criterion) in order to determine the available number of singular values.

Retrieving crosswell wavefields using MDD

Implicit crosswell Green's function representation

Seismic interferometry by MDD is derived from one-way wavefield reciprocity. Considering two seismic states and substituting their properties into a one-way wavefield reciprocity theorem produces the following convolution relation (Wapenaar et al. 2008a):

$$\hat{p}^L(\mathbf{x}_A,\mathbf{x}_S,\omega) = \int_{\partial D_1} \hat{G}^L(\mathbf{x}_A,\mathbf{x},\omega)\hat{p}^L(\mathbf{x},\mathbf{x}_S,\omega)d\mathbf{x}^2 \quad , \qquad (1)$$

where $\hat{p}^L(\mathbf{x}_A,\mathbf{x}_S,\omega)$ indicates an acoustic pressure observed at the receiver position $\mathbf{x}_A$ at well-1 from a physical source placed at the surface at $\mathbf{x}_S$. Similarly, $\hat{p}^L(\mathbf{x},\mathbf{x}_S,\omega)$ indicates the acoustic pressure observed at receiver position $\mathbf{x}$ at well-2 from the physical source at $\mathbf{x}_S$ (see Figure 1). The superscripts "L" indicate decomposed leftward propagating wavefields. $\hat{G}^L(\mathbf{x}_A,\mathbf{x},\omega)$ indicates the crosswell Green's function at receivers in well-1 assuming well-2 as the virtual source positions. Equation 1 states that integrating the multiplication (in the frequency domain) of crosswell Green's functions and observed records at well-2 along all receiver positions gives the observed records at well-1. Derivation of equation 1 is identical to that in Wappenaar et al. (2008a).

Multidimensional deconvolution using SVD

Resolving $\hat{G}^L(\mathbf{x}_A,\mathbf{x},\omega)$ from equation 1 involves MDD. When we consider one receiver position in well-1 $(\mathbf{x}_A)$ and multiple source positions $(\mathbf{x}_S)$, equation 1 can be written in a matrix-form notation (Berkhout, 1982).

$$\hat{\mathbf{P}}^L_{\mathrm{A}} = \hat{\mathbf{G}}^L\hat{\mathbf{P}}^L_{\mathrm{B}}. \qquad (2)$$

Application of MDD to crosswell seismic reflection using SVD

In the case of n sources on the surface and m receivers in each borehole, $\hat{\mathbf{P}}_{\mathrm{B}}^{L}$ is a $m\times n$ matrix whose columns contain $\hat{p}^{L}(\mathbf{x},\mathbf{x}_S,\omega)$ for a fixed source position $(\mathbf{x}_S)$ and variable receiver positions $(\mathbf{x})$ in well-2, i.e., shot gathers, and whose rows contain $\hat{p}^{L}(\mathbf{x},\mathbf{x}_S,\omega)$ for a fixed receiver position $(\mathbf{x})$ and variable source positions $(\mathbf{x}_S)$, i.e., receiver gathers. On the other hand, $\hat{\mathbf{P}}_{\mathrm{A}}^{L}$ is a $1\times n$ row-vector containing $\hat{p}^{L}(\mathbf{x}_A,\mathbf{x}_S,\omega)$ for a fixed receiver position $(\mathbf{x}_A)$ and variable source positions $(\mathbf{x}_S)$. Similarly, $\hat{\mathbf{G}}^{L}$ is a $1\times m$ row-vector containing $\hat{G}^{L}(\mathbf{x}_A,\mathbf{x},\omega)$ for a fixed receiver position $(\mathbf{x}_A)$ and variable borehole source positions $(\mathbf{x})$. When the rank of MDD matrix $\hat{\mathbf{P}}_{\mathrm{B}}^{L}$ is $rank(\hat{\mathbf{P}}_{\mathrm{B}}^{L})=r\le\min[n,m]$, we can use SVD for decomposing $\hat{\mathbf{P}}_{\mathrm{B}}^{L}$ as

$$\hat{\mathbf{P}}_{\mathrm{B}}^{L}=\mathbf{V}_r\boldsymbol{\Delta}_r\mathbf{U}_r^{*}, \tag{3}$$

where $\boldsymbol{\Delta}_r$ is an $r\times r$ diagonal matrix whose diagonal components are non-zero singular values. Now we obtain the pseudoinverse of $\hat{\mathbf{P}}_{\mathrm{B}}^{L}$ using SVD. Hence, the SVD pseudoinverse solution of equation 2 becomes,

$$\hat{\mathbf{G}}_{est}^{L}=\hat{\mathbf{P}}_{\mathrm{A}}^{L}\mathbf{U}_r\boldsymbol{\Delta}_r^{-1}\mathbf{V}_r^{*}. \tag{4}$$

Evaluating equation 4 for all frequencies results in retrieving new spectra of the crosswell Green's function $\hat{G}^{L}(\mathbf{x}_A,\mathbf{x},\omega)$ as a common-receiver gather.

Numerical modeling results

Data acquisition

We applied seismic interferometry by MDD (equation 4) to numerical-modeling data acquired in two parallel boreholes from transient surface sources. The velocity model was inspired from logging P-wave velocity of our field data discussed in the following section. Two vertical boreholes are placed: well-1 (left well) and well-2 (right well) are represented as the receiver arrays in Figure 1 (triangles). Each receiver array consists of 72 receivers starting from 28 m and going to 170 m depth with 2 m intervals. Controlled sources are placed along the free surface. From equation 4, we need only the leftward-propagating wavefield when we want well-2 to contain the virtual source positions. Because our velocity model is 1D in the vertical direction, all wavefields recorded in the boreholes from the sources placed at the right side of well-2 can be regarded as the leftward-going wavefield. The 103 active sources are placed at the free surface along 200 m starting from well-2 with interval of 2 m. Wavefields were calculated using Finite Difference Time Domain (FDTD) method. The source wavelet is a Ricker wavelet with central frequency of 80 Hz. Modeled data was contaminated with Gaussian-distributed noise in order to admit AIC calculation as discussed later. Furthermore, the modeled data was normalized by RMS of the amplitudes at each trace and converted to the frequency domain by Fourier transformation. SVD pseudo inverse solution (equation 4) was applied to each frequency component with the available rank of $\hat{\mathbf{P}}_{\mathrm{B}}^{L}$. Because the modeled data was band-limited, we evaluate equation 4 from 0 Hz to 300 Hz, and the other frequency components are set to be zero in the retrieved data. Inverse Fourier transformation of the retrieved frequency components yields the retrieved crosswell wavefields in the time domain.

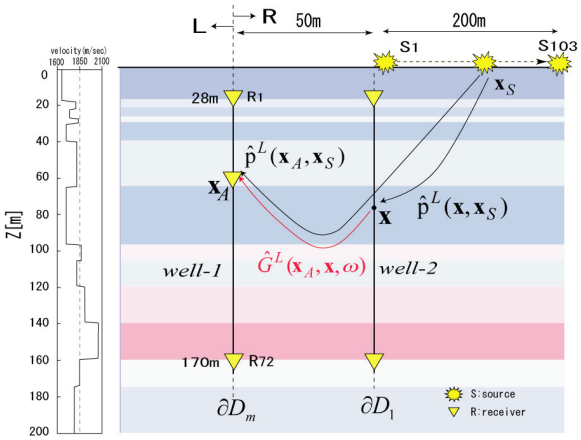

Figure 1 : Velocity model for numerical modeling and source-receiver configuration.

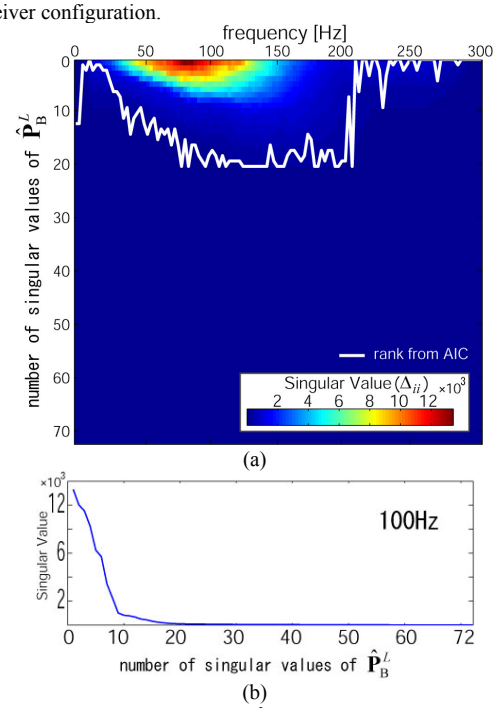

Figure 2 : (a) Singular values of $\hat{\mathbf{P}}_{\mathrm{B}}^{L}$ at each frequency and determined rank from AIC. (b) Singular values of $\hat{\mathbf{P}}_{\mathrm{B}}^{L}$ at 100 Hz.

Application of MDD to crosswell seismic reflection using SVD

Rank determination of the MDD matrix

Singular values of $\hat{\mathbf{P}}_{\mathrm{B}}^{L}$ are calculated at all frequencies (Figure 2a). The columns of Figure 2a show singular values (diagonal components of $\mathbf{\Lambda}_r$) aligned from their maximum value. As $r = rank(\hat{\mathbf{P}}_B^L) \le \min(n,m)$, Figure 2a shows 72 singular values at each frequency. Figure 2b shows singular values at 100 Hz for example. One can see that the first 20 singular values are non zero, however, the remaining 52 singular values are close to zero. This means that the MDD matrix can be recognized as non full-rank matrix. This could be due to the distribution of the active sources. When the surface sources are more widely distributed, the condition of $\hat{\mathbf{P}}_{\mathrm{B}}^{L}$ is expected to be enhanced. In order to determine the rank of $\hat{\mathbf{P}}_{\mathrm{B}}^{L}$ and to obtain a suitable SVD solution in each frequency, we evaluate AIC defined as

$$AIC = m \ln|\sigma|^2 + 2(k+1) \qquad (5)$$

where k is the number of singular values of $\hat{\mathbf{P}}_B^L$ (or rank of $\hat{\mathbf{P}}_B^L$) for computing the pseudoinverse and σ is the variance of the data ($\hat{\mathbf{P}}_{\mathrm{A}}^{L}$) using $\hat{\mathbf{G}}_{est}^{L}$ with k. Suitable number of singular values for $\hat{\mathbf{P}}_B^L$ is determined by minimizing AIC (Akaike, 1974; Matsuoka and Ulrych, 1986). The white broken line in Figure 2a shows the rank k giving minimum AIC in each frequency when using receiver gather $\hat{\mathbf{P}}_{\mathrm{A}}^{L}$ whose receiver is placed at 106 m depth in well-1.

Imaging result via MDD

Using determined ranks from AIC, the crosswell Green's function $\hat{G}^L(\mathbf{x}_A, \mathbf{x}, \omega)$ is retrieved as a receiver gather from equation 4. Figure 3a shows the crosswell receiver gather retrieved from MDD in time domain whose receiver is placed at 106 m depth in well-1. For comparison, furthermore, the crosswell receiver gather from the conventional crosscorrelation (CC) method (Figure 3b) and direct modeling results (Figure 3c) are shown. Figure 3 shows a free-surface reflection (r_1), reflection from the boundary at 160 m (r_2) and reflection from the boundary at 40 m (r_3). Several reflection events (r_1 and r_2) can be recognized in both MDD and CC result. Since MDD retrieves Green's function while CC has as a wavelet the autocorrelation of the wavelet of the active sources, the retrieved events in MDD have higher resolution than those in CC (note that for a better comparison, CC results should be deconvolved with this wavelet). Furthermore, the free-surface reflection (r_1) and the reflection from 40 m (r_3) in MDD are well recognizable compared to those in CC. These two reflection events (r_1 and r_3) are 'downgoing' reflection events. These downgoing events are not well recognizable in CC result (Figure 3b) because the physical sources are localized only on the surface (Minato et al., 2007). From these observations, therefore, we conclude that MDD tends to compensate for the source localization and retrieve not only upgoing events but also downgoing events with better amplitudes. Equation 2 with different receiver gathers for $\hat{\mathbf{P}}_{\mathrm{A}}^{L}$ and $\hat{\mathbf{G}}^{L}$ is handled as a different problem ($\hat{\mathbf{P}}_{\mathrm{B}}^{L}$ is identical for all receiver gathers of $\hat{\mathbf{P}}_{\mathrm{A}}^{L}$ and $\hat{\mathbf{G}}^{L}$). Therefore, rank determination using AIC is evaluated in each focusing receiver gather. To retrieve all crosswell wavefields (all crosswell receiver gathers), we evaluate AIC and apply MDD for all receiver gathers. Hence, the total crosswell data retrieved from the MDD contains 72×72 traces. Kirchhoff depth migration was applied to these crosswell wavefields. Migrated images derived from MDD and from conventional CC are shown in Figure 4. Due to the wide mapping aperture and limited ray coverage, imaged boundaries are dipped toward well positions. One can recognize that the MDD result has higher resolution than CC. Furthermore, shallow boundaries are better imaged

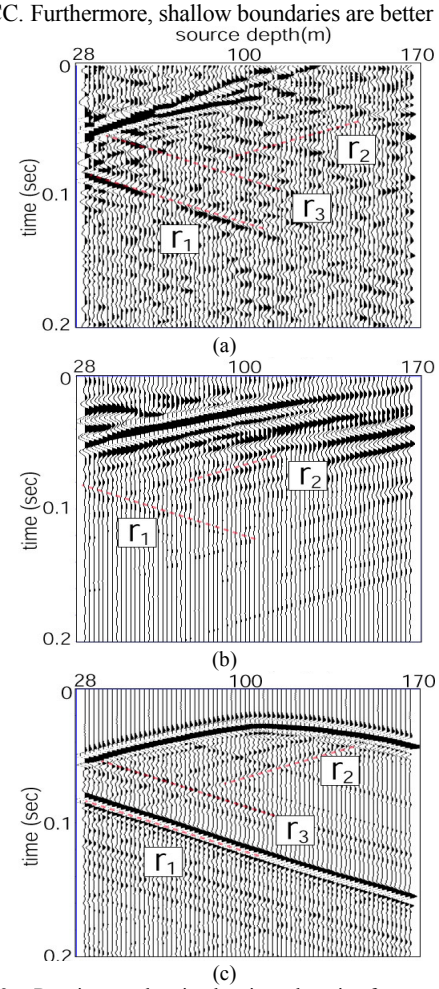

Figure 3 : Receiver gather in the time domain, for a receiver at 106m depth in well-1, constructed from (a) MDD, (b) conventional CC, and (c) direct modeling. The dotted lines r_1, r_2 and r_3 indicate a free-surface reflection, a reflection from the boundary at 160m, and a reflection from the boundary at 40m respectively.

in the MDD result compared with the CC result. This is because the downgoing reflection events are better retrieved using the MDD.

Application to field data

Data acquisition

We applied seismic interferometry by MDD (equation 4) to field data. The receiver arrays configuration in the two boreholes was identical to that of the numerical modeling in the previous section. Crosswell wavefields were retrieved from hydrophone records in the boreholes using transient explosive sources on the surface. Due to the limitation of available area for this experiment, only 13 sources were placed to the right from well-2 with 5 m interval. The acquired data was F-K filtered to remove S-waves in order to handle only P-waves, and normalized by RMS of amplitudes. Since the horizontal reflection boundaries are dominant in this field (Minato et al., 2007), wavefield separation into leftward going wavefield was not applied (as explained in the numerical-modeling section).

MDD and imaging

Figure 5 shows the calculated singular values of $\hat{\mathbf{P}}_{\mathrm{B}}^{L}$. As $r = rank(\hat{\mathbf{P}}_{B}^{L}) \le \min(n,m)$, Figure 5 shows 13 singular values at each frequency. The white broken line indicates the rank of $\hat{\mathbf{P}}_{\mathrm{B}}^{L}$ determined from AIC using a receiver gather at 106 m depth. Using these ranks, the crosswell receiver gather was retrieved. Figure 6 shows migrated subsurface images using the total crosswell wavefield data derived from MDD (Figure 6a), from conventional CC (Figure 6b) and logging P-wave velocity (Figure 6c). Just like with the numerical modeling, the MDD result has higher resolution than CC; the shallow boundaries are well imaged in MDD results. Furthermore, the imaged reflection boundaries are in a good agreement with the logging P-wave velocity (Figure 6c).

Conclusion

We applied seismic interferometry by multidimensional deconvolution (MDD) to crosswell geometry to retrieve crosswell impulse responses using numerical-modeling and field data. We adopted singular value decomposition (SVD) pseudoinverse solution to achieve MDD. The singular value matrix $\hat{\mathbf{P}}_{\mathrm{B}}^{L}$ of the matrix to be inverted is not of full rank. To determine the rank for the SVD pseudoinverse solution, Akaike's information criterion (AIC) is evaluated. The MDD results exhibit higher resolution and improved amplitudes compared with the results from seismic interferometry by crosscorrelation. We used the results retrieved from the MDD to obtain an image of the subsurface. This image was in a good agreement with a P-wave velocity log of the subsurface.

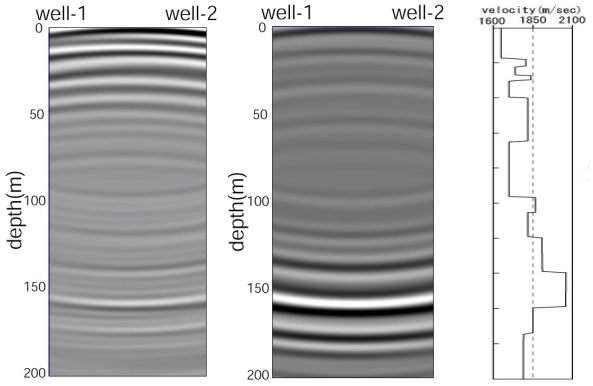

Figure 4 : Imaging results from (a) MDD, (b) conventional CC, and (c) velocity model.

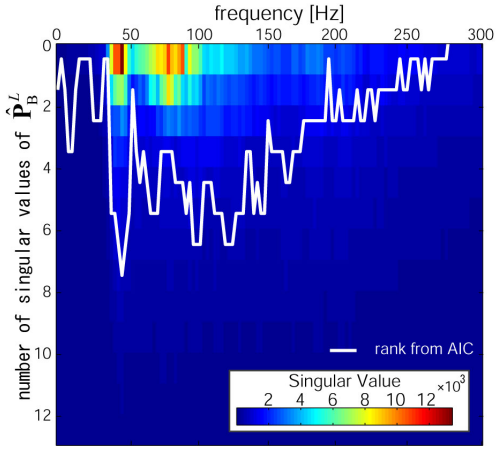

Figure 5 : Singular values of $\hat{\mathbf{P}}_{\mathrm{B}}^{L}$ at each frequency and determined rank from AIC.

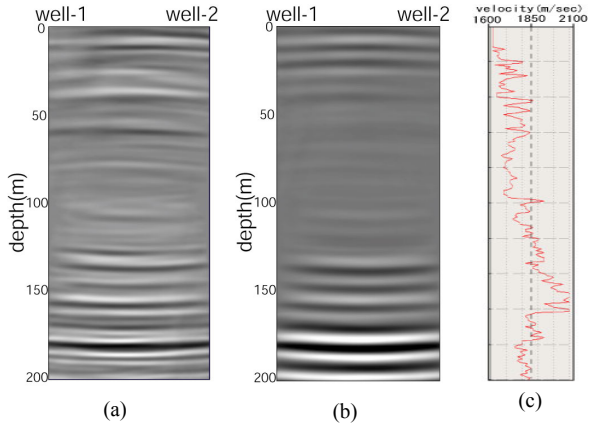

Figure 6 : Imaging results from (a) MDD, (b) conventional CC, and (c) logging P-wave velocity

Akaike, H., 1974 : A new look at the statistical model identification, IEEE Trans. Automat. Contr., AC-19, 716-723.

Bakulin, A. and R., Calvert, 2006 : The virtual source method Theory and case study, Geophysics, 71, SI139-SI150.

Berkhout A. J., 1982 : Seismic Migration. Imaging of Acoustic Energy by Wave Field Extrapolation. Elsevier.

Matsuoka, T. and Ulrych, T., 1986 : Information theory measures with application to model identification, IEEE Trans. Acoust. Speech Signal Process., 34, 511-517, 1986

Minato, S., K. Onishi, T. Matsuoka, Y. Okajima, and J. Tsuchiyama, 2007 : Cross-well seismic survey without borehole source, SEG, Expanded abstracts, 1357-1361.

Schuster G. T., J. Yu, J. Sheng, and J. Rickett, 2004 : Interferometric/daylight seismic imaging. Geophysical Journal International, 157, 838-852.

Snieder, R., 2004 : Extracting the Green's function from the correlation of coda waves: A derivation based on stationary phase. Physical Review E 69, 046610.

Wapenaar, K., 2004 : Retrieving the elastodynamic Green's function of an arbitrary inhomogeneous medium by cross correlation, Physical Review Letters, 93, 254301.

Wapenaar, K., and J. Fokkema, 2006 : Green's function representations for seismic interferometry, Geophysics, 71, SI33-SI46

Wapenaar, K., E. Slob, and R. Snieder, 2008a : Seismic and electromagnetic controlled-source interferometry in dissipative media, Geophys. Prosp., 56, 419-434.

Wapenaar, K., J. van der Neut, and E. Ruigrok, 2008b : Passive seismic interferometry by multidimensional deconvolution, Geophysics, 73, A51-A56.